

# DETECTION OF NON-GAUSSIANITY ON THE SPHERE USING SPHERICAL WAVELETS

J.E. GALLEGOS<sup>1</sup>, J.L. SANZ<sup>1</sup>, E. MARTÍNEZ-GONZÁLEZ<sup>1</sup>,  
F. ARGÜESO<sup>2</sup> & CAYÓN, L.<sup>1</sup>

<sup>1</sup>*Instituto de Física de Cantabria, Santander E39006, SPAIN*

<sup>2</sup>*Department of Mathematics, Universidad de Oviedo, Oviedo E33007, SPAIN*

We present results showing the efficiency of the spherical Mexican Hat wavelet in detecting non-Gaussian CMB features on the sphere. We compare its performance with that of the spherical Haar wavelet for two non-Gaussian fields artificially generated using the Edgeworth expansion to introduce skewness and kurtosis respectively. By combining all the information present in all the wavelet scales with the Fisher discriminant, we find that the spherical Mexican Hat wavelets are clearly superior to the spherical Haar wavelets. The former can detect levels of the skewness and kurtosis of  $\approx 1\%$  for  $33'$  resolution. The introduction of instrumental white noise in the maps,  $S/N = 1$ , does not change the main conclusion of this work. These results are relevant to test the Gaussian character of CMB and therefore the standard inflationary scenario.

## 1 Introduction

Establishing the statistical character of the CMB fluctuations will provide crucial evidence about the physical origin of the primordial density fluctuations in the early universe. Simple inflationary models predict a homogeneous and isotropic Gaussian random field for the temperature fluctuations. On the contrary, non-standard inflation and cosmic defects generically predict non-Gaussian random fields. Relevant information on the non-Gaussian nature of the data which is otherwise hidden in the temperature fluctuation maps can be extracted using specific methods. These methods are grouped by the spaces (real, Fourier,...) in which they act. As it is often pointed out, wavelets are a very useful tool for data analysis due to its space-frequency localisation. It has been already demonstrated in many applications in a wide variety of scientific fields. In particular in relation to the CMB the COBE-DMR data has been studied with several wavelet bases acting on the faces of the quad-cube COBE pixelisation<sup>12,11,1</sup>. More appropriate analyses should involve the use of spherical wavelets as in Tenorio *et al.*<sup>14</sup>. More recently Barreiro *et al.*<sup>3</sup> and Cayón *et al.*<sup>6</sup> have convolved the COBE-DMR data with spherical wavelets in the HEALPIX pixelisation<sup>9</sup> to test the Gaussianity of these data. Those works used the Spherical Haar Wavelet (SHW) and the Spherical Mexican Hat Wavelet (SMHW), respectively.

## 2 The MEXHAT on $S^2$

For CMB analyses we are interested in the extension of these isotropic wavelets to the sphere. Recently, Antoine & Vanderghyest<sup>2</sup> have followed a group theory approach to deal with this

problem. This extension incorporates four basic properties: a) the basic function is a compensated filter, b) translations, c) dilations and d) Euclidean limit for small angles. They conclude that the stereographic projection on the sphere is the appropriate one to translate the wavelet properties from the plane to the sphere. A particular example is the MEXHAT wavelet defined by

$$\Psi(\theta; R) = \frac{1}{(2\pi)^{1/2} R N} \left[ 1 + \left(\frac{y}{2}\right)^2 \right] \left[ 2 - \left(\frac{y}{R}\right)^2 \right] e^{-y^2/2R^2}, \quad (1)$$

$$N(R) \equiv \left( 1 + \frac{R^2}{2} + \frac{R^4}{4} \right)^{1/2}, \quad y \equiv 2 \tan \frac{\theta}{2}. \quad (2)$$

We remark that the normalization constant has been chosen such that  $\int d\theta d\phi \sin\theta \Psi^2(\theta; R) = 1$ . This is the wavelet we are going to use to analyze non-Gaussianity associated to different models. We comment that the stereographic projection of the MEXHAT wavelet has been recently used to analyze maps of the cosmic microwave background radiation (CMB) <sup>6</sup>.

### 3 Spherical Haar Wavelet

SHW were introduced by Sweldens<sup>13</sup> as a generalization of planar Haar wavelets to the pixelised sphere. They are orthogonal and adapted to a given pixelisation of the sky which must be hierarchical, contrary to the SMHW which are non-orthogonal and redundant. However they are not obtained from dilations and translations of a mother wavelet, contrary to planar Haar wavelets and SMHW. As for the planar Haar wavelets, they possess a good space-frequency localisation. However, their frequency localisation is not as good as that of the SMHW. The SHW decomposition is based on one scaling  $\phi_{j,k}$  and three wavelet functions  $\psi_{m,j,k}$  at each resolution level  $j$  and position on the grid  $k$ . For HEALPix the resolution is given in terms of the number of divisions in which each side of the basic 12 pixels is divided,  $N_{side} = 2^{j-1}$ . Thus, for level  $j$  the total number of pixels with area  $\mu_j$  is given by  $n_j = 12 \times 4^{j-1}$ . Each pixel  $k$  at resolution  $j$ ,  $S_{j,k}$  is divided into four pixels  $S_{j+1,k_0}, \dots, S_{j+1,k_3}$  at resolution  $j+1$ . The generation of coefficients start with the original map, finest resolution  $j = J$ , for which the coefficients  $\lambda_{J,k}$  are identified with the temperature fluctuation at pixel  $k$ . Finally, from the definition of the SHW it is easily seen that this wavelet is not rotationally invariant, contrary to the SMHW.

### 4 Non-Gaussian simulations

Here the spherical wavelets will be tested against non-Gaussian simulations of artificially specified moments that will be assumed to be small. In this case a useful way to construct non-Gaussian distributions is by perturbing the Gaussian one through a sum of moments, the Edgeworth expansion. The Edgeworth expansion can be obtained from the characteristic function  $\phi(t)$  by considering the linear terms in the cumulants and performing the inverse Fourier transform to recover the density function  $f(x)$ :

$$f(x) = G(x) \left\{ 1 + \sum_{n=3}^{\infty} \frac{k_n}{n! 2^{n/2}} H_n\left(\frac{x}{\sqrt{2}}\right) + O(k_n k_{n'}) \right\}, \quad (3)$$

where  $H_n$  is the Hermite polynomial. Since wavelet coefficients represent linear transformations of the original data, in the case of a Gaussian distribution the wavelet coefficients remain Gaussian distributed. This a very nice property of wavelets and all we have to do to test Gaussianity in wavelet space is to look for deviations from normality. However, for the case of the sphere any given pixelisation scheme will introduce biases. The specific bias introduced will depend on,

Table 1: Power of the Fisher discriminant at 1% significance level

	Moment <sup>1</sup> $\times 10^{-2}$	SMHW P(%)	SHW P(%)	Temperature P(%)
SKEWNESS	0.9(2.4)	66.8	1.51	2.51
	1.6(2.3)	100	7.09	4.67
	4.6(2.4)	100	36.12	36.85
	6.9(2.4)	100	78.46	73.60
KURTOSIS	0.3(2.6)	15.35	3.00	1.42
	0.8(2.7)	86.89	9.00	3.40
	1.1(2.7)	98.10	16.11	4.90
	1.4(2.6)	99.90	28.43	3.50

<sup>1</sup> Mean value obtained in the analysed maps. The standard deviation is given within parenthesis.

for instance, whether the pixels are not of equal area or the distances between one pixel and its neighbours vary with the position on the sphere. This bias produces a peaked distribution with respect to a Gaussian and therefore a positive kurtosis in the three details of the SHW coefficients even for temperature realizations derived from normal distributions. In the case of the SMHW we only have a type of coefficients for each scale. Since this is a continuous, rotationally invariant wavelet -and thus not adapted to the pixelisation- no bias is produced in this case.

## 5 Discriminating power

We use as test statistic the Fisher linear discriminant function<sup>8,7</sup>. The Fisher discriminant<sup>4</sup> is a linear function of the data that maximizes the distance between the two pdf's,  $g(t|H_0)$  and  $g(t|H_1)$ , such a distance defined as the ratio  $(\tau_0 - \tau_1)^2 / (\Sigma_0^2 + \Sigma_1^2)$ .  $\tau_k$  and  $\Sigma_k^2$ ,  $k = 0, 1$ , are the mean and the variance of  $g(t|H_k)$ , respectively. The Fisher discriminant is given by:  $t(\vec{x}) = (\vec{\mu}_0 - \vec{\mu}_1)^T W^{-1} \vec{x}$ , with  $W = V_0 + V_1$  and  $V_k$  the covariance matrix and  $\vec{\mu}_k$  the mean values of  $f(\vec{x}|H_k)$ . In the particular case that  $f(\vec{x}|H_0)$  and  $f(\vec{x}|H_1)$  are both multidimensional Gaussians with the same covariance matrix, the Fisher discriminant is equivalent to the likelihood ratio.

In Figure 1 (top), we show the deviations from Gaussianity for two non-Gaussian models for the first five resolution levels of the wavelets. It is clear that the performance of the SMHW is much better than that of the SHW. In Figure 1 (bottom), we show, as an example, the pdfs of the statistic  $t$  for one value of skewness of the non-Gaussian models. It is clear that the SMHW is able to distinguish between the Gaussian and non-Gaussian models much better than the SMW. In table 1 the power  $p$  of the Fisher discriminant constructed from the skewness or kurtosis of the SMHW, SHW and temperature is given for several values of the cumulants. For the case of the temperature of the map the statistic is given directly by its cumulants. Again, the performance of the SMHW is superior to the SHW and the temperature in all cases.

In order to know the effect of instrumental noise (white) on the discriminating power of the spherical wavelets we have also added noise to the temperature maps with an amplitude equals to the signal,  $S/N = 1$ . For this case, the first resolution scale is the most affected and now the second scale is the most relevant for discrimination between models. The noise narrows the separation between distributions as compared to the no-noise case (bottom Figure 1). The SMHW is still able to discriminate with a high power for the skewness model with a skewness value in the analysed map of 1.1%. For the kurtosis model, the addition of noise with the same amplitude than the signal, reduces the level of kurtosis in the analysed map from 1.4% to 0.2%, a level too low to be detectable. The main conclusion of this work is that the SMHW bases are much more efficient to discriminate between Gaussian and non-Gaussian models with either skewness or kurtosis present in the CMB maps than the Spherical Haar Wavelet (SHW) ones. For a more complete description of the method and results see Martínez-González *et al.*<sup>10</sup>

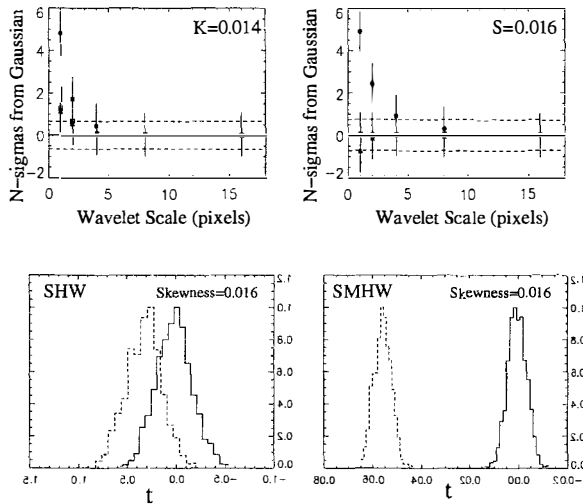


Figure 1: TOP: Comparison of Kurtosis and Skewness for the Spherical Mexican Hat wavelet (black circle) and the Spherical Haar Wavelet details. Each point represents the number of sigmas deviated from the Gaussian model. BOTTOM: Fisher discriminant for a skewness model from Spherical Haar Wavelet and Spherical Mexican Hat Wavelet compared to the Gaussian model (solid line).

## References

1. Aghanim, N., Forni, O. & Bouchet, F.R. *Astronomy & Astrophysics* **365**, 41 (2001)
2. Antoine, J.-P. & Vandergheynst, P. *J. Math. Phys.* **39**, 3987 (1998)
3. Barreiro, R.B., Hobson, M.P., Lasenby, A.N., Bay, A.J., Górski, K.M. & Hinshaw, G. *MNRAS* **318**, 475 (2000).
4. Barreiro, R.B. & Hobson, M.P. *MNRAS* **327**, 813 (2001)
5. Barreiro, R.B., Martínez-González, E. & Sanz, J.L. *MNRAS* **322**, 411 (2001)
6. Cayón, L., Sanz, J.L., Martínez-González, E., Banday, A.J., Argüeso, F., Gallegos, J.E., Gorski, K.M. & Hinshaw, G. *MNRAS* **326**, 1243 (2001).
7. Cowan, G., *Statistical Data Analysis*, Oxford University Press (1998)
8. Fisher R.A., *Ann. Eugen.* **7**, 179 (1936); reprinted in "Contributions to Mathematical Statistics", 1950, John Wiley, New York
9. Górski, K.M., Hivon, E. & Wandelt, B.D. *Proceedings of the MPA/ESO Conference on Evolution of Large-Scale Structure: from Recombination to Garching. astro-ph/9812350*, (1999)
10. Martínez-González, E., Gallegos, J.E., Argüeso, F., Cayón, L. & Sanz, J.L., accepted for publication in *MNRAS astro-ph/0111284*, (2002).
11. Mukherjee, P., Hobson, M.P. & Lasenby, A.N. *MNRAS* **318**, 1157 (2000)
12. Pando, J. Valls-Gabaud, D., Fang, L.Z. *Phys.Rev.Lett.* **81**, 4568 (1998)
13. Sweldens, W., *Applied Comput. Harm Anal.* **3**, 1186 (1996)
14. Tenorio, L., Jaffe, A.H., Hanany, S. & Lineweaver, C.H. *MNRAS* **310**, 823 (1999)
15. Wu, J.H.P. et al. *Phys.Rev.Lett.* **87**, 251303 (2001)